Energy transfer from colloidal nanocrystals into Si substrates studied via photoluminescence photon counts and decay kinetics

H. M. Nguyen,[1] O. Seitz,[2] Yu. N. Gartstein,[1] Y. J. Chabal,[2] and A. V. Malko[1,*]

[1]*Department of Physics, The University of Texas at Dallas EC36, Richardson, Texas 75080, USA*
[2]*Department of Materials Science, The University of Texas at Dallas, Richardson, Texas 75080, USA*
**Corresponding author: anton.malko@utdallas.edu*

Received June 3, 2013; accepted July 26, 2013;
posted July 31, 2013 (Doc. ID 191399); published August 16, 2013

We use time-resolved photoluminescence (PL) kinetics and PL intensity measurements to study the decay of photoexcitations in colloidal CdSe/ZnS nanocrystals grafted on SiO_2 – Si substrates with a wide range of the SiO_2 spacer layer thicknesses. The salient features of experimental observations are found to be in good agreement with theoretical expectations within the framework of modification of spontaneous decay of electric-dipole excitons by their environment. Analysis of the experimental data reveals that energy transfer (ET) from nanocrystals into Si is a major enabler of substantial variations in decay rates, where we quantitatively distinguish contributions from nonradiative and radiative ET channels. We demonstrate that time-resolved PL kinetics provides a more direct assessment of ET, while PL intensity measurements are also affected by the specifics of the generation and emission processes.

OCIS codes: (300.6500) Spectroscopy, time-resolved; (250.5230) Photoluminescence; (260.2160) Energy transfer; (160.4760) Optical properties.
http://dx.doi.org/10.1364/JOSAB.30.002401

1. INTRODUCTION

Energy transfer (ET) is an important phenomenon that can substantially modify the lifetime of excited states of various fluorophores [1]. One of the well-characterized mechanisms of ET is Förster (or fluorescence) resonance energy transfer (FRET) that has become a frequently used photophysical tool in analytical chemistry and biological research [1–3]. FRET is a nonradiative (NR), dipole–dipole interaction assisted [1,4,5], process of ET between proximal energy donor and energy acceptor species. Common FRET techniques rely on measurements of photoluminescence (PL) quenching of the donor emission and (to a lesser extent) enhancement of the PL of the acceptor. The advent of single molecular (sm) detection methods led to the widespread use of the sm-FRET techniques [1] to obtain accurate information about fluorophores' locations due to the sensitive, $\propto 1/r^6$, dependence of FRET on separation distance r between two small donor and acceptor species.

ET can also become a crucial enabler in hybrid nanostructures judiciously designed for optoelectronic applications [6,7] and involving various organic and inorganic components with the roles of energy donor and acceptor [8–13]. In photovoltaics-oriented hybrids, it is envisioned that the incident solar light is efficiently harvested in its strongly absorbing component followed by energy (exciton) diffusion and transfer across the interface into the other, high carrier mobility, component where the separation and transport of charge carriers takes place. The idea of external NRET-sensitization of inorganic semiconductors for photovoltaic (PV) applications, probably first discussed by Dexter [14], received a renewed attention recently with the help of colloidal nanocrystal quantum dots (NQDs) as a different type of the sensitizer [8–12]. NQDs possess attractive properties and serve as good light absorbers and quantum emitters; they are photostable and their size-dependent band gaps allow for easy tuning of the PL emission wavelength. NRET with NQD fluorophores has been under studies in biological systems [1,3] as well as in dense assemblies [15].

Our recent experiments have demonstrated that photoexcited NQDs can act as efficient energy donors for adjacent silicon materials, including both thick substrates [10,12] and ultrathin (~50–300 nm) Si nanomembranes [11]. Hybrid nanostructures combining NQDs with crystalline Si layers therefore offer a potential for development of novel ET-based thin-film PV devices. Our analysis of the PL decays for NQDs in the vicinity of Si substrates in fact identified and distinguished two ET mechanisms: in addition to NRET, we found that radiative energy transfer (RET) can be a substantial contributor, particularly toward near-infrared wavelengths [12]. While NRET corresponds to the direct production of electron-hole pairs [16] in Si by the dipolar field of NQD excitons, efficient RET is enabled by preferential decay of excitons into photonic modes that propagate only within substrates (waveguiding modes in thin layers [5]). These mechanisms have different dependence on NQD distance r from the substrate: NRET exhibits $\propto 1/r^3$ scaling typical for transfer into an underlying bulk array of acceptors [15,17,18] and is estimated to be effective over distances of several nanometers. RET, however, can be a considerably longer-range process. The rationalization of experimental observations within this picture follows from a good agreement with theoretical calculations [11,12] employing the frequency-dependent dielectric

properties of Si [19]. The NQD-on-Si-substrates systems thus also make an interesting "case study" for a well-known problem of modification of radiative lifetimes of electric-dipole emitters in the vicinity of polarizable environments [5,17,20]. Various metallic and semiconductor nanostructures are studied nowadays for purposes of "radiative decay engineering" [1] and even for engineering of spontaneous emission patterns [21].

In this paper, we extend our earlier studies of ET from colloidal CdSe/ZnS nanocrystals (vacuum peak emission wavelength $\lambda_0 \simeq 565$ nm) into Si substrates by providing a detailed comparison of time-resolved measurements of NQD PL kinetics with measurements of NQD PL emission quenching. The comparison is made for a multitude of samples with a wide range (approaching $\sim 0.7\lambda_0$) of *in situ* controlled thicknesses d of the SiO_2 spacer layer separating NQDs from the Si substrate. In this way, we are able to better distinguish and characterize ET mechanisms and particularly to follow RET at larger separations. We also illustrate an important methodological point that the interpretation of the PL intensity data in such layered systems requires special care as photon counts can be affected not only by ET but also by the specifics of the optical generation rates and emission collection. This is unlike typical experimental conditions in solution environments, where the rate of molecular excitation and proportion of the collected PL emission are largely independent of the molecular arrangement. Indeed, the interference effects in multilayered structures modify the electric field intensity at the surface thereby modifying the number of photogenerated NQD excitons. The radiative emission pattern is also well-known to depend on the geometry [5], and different relative amounts of emission may be collected with the same objective. We employ the macroscopic electrodynamics framework [5] to evaluate various decay channels of NQD excitons and show variations of the angular PL emission pattern as a function of thickness d of the spacer layer. A good correspondence with the amount of the experimentally observed PL is achieved when the interference of the excitation field is taken into account that modulates the number of the photogenerated NQD excitons. PL lifetime changes, on the other hand, are not affected by these peculiarities and thus serve as a more direct quantitative measure of ET processes.

2. EXPERIMENTAL DETAILS

Bulk crystalline Si substrates were first thermally oxidized in the clean room environment to create a thick (400 nm) SiO_2 layer. The substrate was then vertically dipped into 1% HF etching solution and removed from the solution in a step-like fashion, resulting in SiO_2 terraces with a variety of thicknesses d of the spacer and several millimeters width each. For each step, thickness d was measured via spectroscopic ellipsometry using a standard model of the SiO_2 layer on silicon. The top surfaces were subsequently functionalized as previously described [22–24] to eliminate surface defects and achieve a controlled attachment of NQDs. The functionalization is based on two approaches depending on the starting surface. For oxide-free Si surfaces, a hydrosilylation reaction is performed using ethyl undecylenate molecules, which leads to to a carboxylic-acid-terminated alkyl chain monolayer after transformation of the head groups [22]. For silicon oxide (SiO_2) or pure glass surfaces, the freshly cleaned samples are immersed in a preheated (70°C) anhydrous toluene solution containing 0.2% of triethoxysilyl undecanal (C11-Ald) molecules for 12 h in a recirculation glove box (anhydrous conditions). Water soluble colloidal CdSe/ZnS NQDs emitting at $\lambda_0 \simeq 565$ nm are purchased from Invitrogen [Qdot 565 ITK amino (PEG), # Q21531MP] and used as received. Their optical properties are well characterized by the manufacturer and the in-home measured emission spectrum is available in [10]. The attachment of NQDs is performed differently depending on the head groups: (a) for the carboxyl terminated head group, the sample is immersed in an MES (2-morpholinoethanesulfonic acid) solution containing EDC [1-ethyl-3-(3-dimethylaminopropyl) carbodiimide] (0.8 mg/ml) and with NQD concentration of 15 nM; (b) for the aldehyde terminated head group, the sample is exposed to an NQD solution containing some sodium cyanoborohydride (5 mM). The measured ellipsometric thicknesses of SAM molecules employed in these attachments are 1.5 nm and 2 ± 0.2 nm. The chemistry of our linkers ensures their direct attachment to the NQD body surface resulting thus in the center of NQD to the top surface distances of approximately 3.7 and 4.2 nm, respectively. As discussed in our previous work [10,12], the concentrations used correspond to submonolayer NQD coverages in order to avoid ET effects between NQDs that typically complicate the data interpretation. The samples are left for 90 min for adsorption, rinsed at least twice with deionized water and dried under the N_2 gas.

PL lifetime and intensity measurements were performed in the microscope-based photoluminescence (μ PL) system. Samples were excited by 400 nm laser pulses from a pulse-picked, frequency doubled femtosecond Ti:sapphire oscillator (Coherent MIRA). The pump power was adjusted such that one laser pulse excited less than 0.1 exciton per NQD on average. Low pumping power allowed us to eliminate the possibility of exciton–exciton interaction effects. A laser beam was focused on the sample by an Olympus air microscope objective (40×, 0.6 NA). The PL signal emitted into the collection aperture of the objective lens (full collection angle of 73.7 degrees) was collected and sent to the detection system, see Fig. 1. The collected emission passes through a spectrometer and is directed either to a CCD camera for a spectral analysis or to a sensitive photon detector (MicroPhoton Devices) for the wavelength-dependent PL lifetime detection. PL decays were collected via the time-correlated single-photon counting (TCSPC) performed on board of Pico300E photon counting hardware (PicoQuant GmbH). The overall time resolution was better than 50 ps. All measured PL lifetimes for NQDs grafted on Si and SiO_2 surfaces are well fitted with monoexponential curves, indicating a high uniformity of NQD environments and attesting to the high-quality of the commercial NQDs and nearly perfect grafting method that electronically passivates the surface. Measurements of ET processes can thus proceed unobscured by extraneous decay channels such as the charge carrier trapping typical for NQDs placed on untreated surfaces.

3. RESULTS AND DISCUSSION

It is well recognized that the spontaneous decay of an excited species depends on the local density of electromagnetic modes which can be strongly affected by the environment [5], hence the "radiative decay engineering" [1]. The

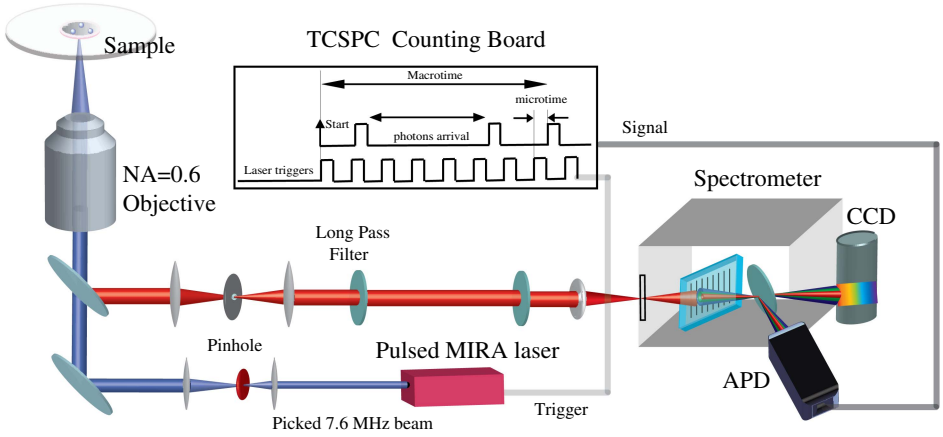

Fig. 1. Schematics of the microscope-based TCSPC experiment used to study PL from NQDs on various substrates.

environment also influences the angular patterns of spontaneous emission observed in PL experiments. The subject has been extensively studied since original Sommerfeld's treatment of the emission by an antenna located near the earth's surface [25,26]. A powerful macroscopic electrodynamics framework has been developed to evaluate electromagnetic decay rates and emission patterns for oscillating dipole emitters in the environments characterized by their frequency ω-dependent complex dielectric functions $\epsilon(\omega) = \epsilon'(\omega) + i\epsilon''(\omega)$. This description has been applied to dipoles in different geometries and media that compares well to experimental data [5,17,27]. For weak exciton-field coupling, the results obtained in the quantum picture of the exciton decay due to fluctuations of the electromagnetic field are identical to those obtained with classical dipoles (Section 8.4 of [5]). Particularly many explicit results have been derived for stratified media (see, e.g., [5,17,28]), which is exactly the case for our experimental geometries. For the reader's convenience and logical consistency, we provide below a brief exposition of some results that are relevant for the discussion of salient features of our experimental observations displayed in Figs. 2 and 4.

Describing the NQD exciton as an ideal point electric-dipole emitter (effective dipole transition moment $\mathbf{p}$) at the NQD center, its decay in vacuum is purely radiative, with the lifetime τ_0 and decay rate $\Gamma_0 = 1/\tau_0$ known to be

$$\Gamma_0 = \frac{k_0^3 |\mathbf{p}|^2}{3\pi\epsilon_0\hbar}, \tag{1}$$

where $k_0 = \omega/c = 2\pi/\lambda_0$ is the emission wavenumber [5]. This decay rate relates to the corresponding power P_0 emitted by a classical dipole. If the dipole is positioned at distance z above a layered substrate, its electromagnetic decay rate is modified to Γ found from

$$\Gamma/\Gamma_0 = 1 + I(0,\infty), \tag{2}$$

$$I(a,b) = \mathrm{Re}\int_a^b \frac{sds}{2\sqrt{1-s^2}}[(2s^2-1)r^{(p)}(s) + r^{(s)}(s)] \times \exp\left(2ik_0 z\sqrt{1-s^2}\right). \tag{3}$$

(The decay rate of a dipole generally depends on its orientation; Eq. (3) is a result of averaging Eq. (10.26) of [5] over random orientations.) Here, $r^{(s)}$ and $r^{(p)}$ are the reflection coefficients for respectively s- and p-polarized waves [5] that contain information on the dielectric properties of the

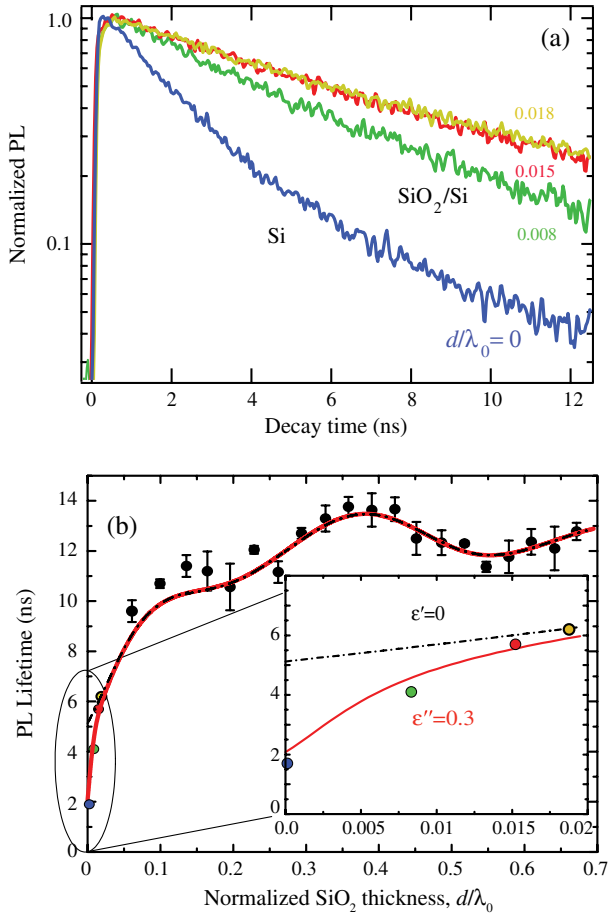

Fig. 2. (a) Examples of NQD PL decays on bare Si and on SiO_2 – Si substrates with thin spacer layers as indicated with values of their normalized thickness d/λ_0. The corresponding PL lifetimes extracted from mono-exponential fits to these decay curves are shown by color-coordinated dots in the inset on panel (b). (b) Measured NQD lifetimes (black dots) as a function of the normalized thickness d/λ_0 of the SiO_2 layer over an extended range of thicknesses. The black dashed–dotted line shows the result of calculations as per Eq. (2) with silicon's $\epsilon'' = 0$, while the red solid curve with $\epsilon'' = 0.3$. The inset displays an expanded view for very thin spacers where NRET contribution is significant.

substrate. In our case the substrate structure involves two interfaces: air/SiO_2 and SiO_2/Si, as taken into account for calculation of reflection and transmission coefficients. Upon reflection/refraction at planar interfaces, the in-plane (parallel to the interface) components of the wave vector are conserved. The integration variable s in Eq. (3) relates magnitude $k_\parallel$ of those in-plane components to the vacuum wave number k_0: $k_\parallel(s) = sk_0$. Consequently, the normal component of the wave vector k_{zi} in each of the layered spatial regions (index i) is determined by the dielectric function ϵ_i of that layer

$$k_{zi}^2(s) = (\epsilon_i - s^2)k_0^2. \tag{4}$$

For our weakly-absorptive ($\epsilon'' \ll \epsilon'$) dielectric SiO_2 – Si substrates, the integration range in Eq. (2) can be meaningfully separated into parts limited by different values of refraction indices $n_i(\simeq\sqrt{\epsilon_i'})$ of the layers, allowing one to distinguish between "propagating" [real or nearly real k_{zi} values as per Eq. (4)] and evanescent (imaginary k_{zi} values) character of the waves in the respective spatial regions. In our computational illustrations below, we adopt the values of refraction indices $n_G = 1.5$ in SiO_2 and $n \simeq 4.04$ in Si. The latter quantity corresponds to $\epsilon' = 16.3$ and $\epsilon'' = 0.3$ used here as representative values for silicon's dielectric function in the spectral region of our NQD emission line [19].

Equation (4) makes it clear that contribution

$$1 + I(0,1) \tag{5}$$

to Eq. (2) describes the decay into photons with the propagating character in the whole space ("allowed light" in the parlance of [5]). On the other hand, contribution

$$I(1,n) \tag{6}$$

describes the decay into the electromagnetic modes whose fields are evanescent outside of the substrate ("forbidden light") but would have the propagating character in Si. Of course, the "propagating" modes would in reality experience absorption in Si due to a finite value of its ϵ''. It is, however, important to emphasize that the decay channels (5 and (6) are radiative: they exist for $\epsilon'' = 0$ and in fact do not practically change for small finite values of ϵ''.

A very different type of decay, however, corresponds to contribution

$$I(n,\infty) \tag{7}$$

in Eq. (2). Evidently, by Eq. (4), there are no propagating electromagnetic modes corresponding to this range of variable s. Contribution (7) would vanish for $\epsilon'' = 0$ and is practically proportional to ϵ'' for the small absorption. It thus describes a purely nonradiative process due to dissipative losses [5,7] induced by the electrostatic-like near field of the dipole in Si.

More detail and insight for the radiative processes are obtained in their angular emission patterns that we illustrate in Figs. 3 and 4. Upon integration over the azimuthal angle ϕ and averaging over random dipole orientations, Eq. (10.43) of [5] yields the following expressions for the power $p(\theta)$ emitted into the polar angle sin $\theta d\theta$. For the emission "up," into the air semi-space, one derives

$$\frac{p_\uparrow(\theta)}{P_0} = \frac{1}{2} + \frac{|r^{(p)}|^2 + |r^{(s)}|^2}{4} + \frac{1}{2}\mathrm{Re}[(r^{(s)} - \cos 2\theta r^{(p)})e^{2ik_0 z\cos\theta}]. \tag{8}$$

For the emission "down," into the Si semi-space, the result is

$$\frac{p_\downarrow(\theta)}{P_0} = \frac{n^3\cos^2\theta}{4|1-\alpha|}e^{-2k_0 z\mathrm{Im}\left(\sqrt{1-\alpha}\right)} \times [|t^{(p)}|^2(|1-\alpha| + \alpha) + |t^{(s)}|^2], \tag{9}$$

where $\alpha = n^2\sin^2\theta$. Equations (8) and (9) feature reflection, $r^{(s)}$ and $r^{(p)}$, and transmission, $t^{(s)}$ and $t^{(p)}$, coefficients as functions of angle θ in the corresponding emission directions. Equation (9) clearly shows the significance of critical angle $\theta_1 = \arcsin(1/n) \simeq 14.3°$. Another relevant angle $\theta_2 = \arcsin(n_G/n) \simeq 21.8°$ arises in the context of the transmission coefficients t through the spacer layer.

Figure 2(a) shows few representative PL decay traces for NQDs grafted on bare Si and on SiO_2 – Si substrates with thin SiO_2 spacer layers. We have extracted decay lifetimes from mono-exponential fits to such traces for a variety of spacers and plotted them as a function of the normalized spacer thickness, d/λ_0, in Fig. 2(b). The observed variation of lifetimes should be compared with lifetime $\tau_G \simeq 12.8$ ns measured [10] for NQDs on the reference glass substrate, $d \to \infty$. Applying the model description of Eq. (2) for the ratio of decay lifetimes on our SiO_2 – Si samples and on the reference glass substrate, we can now generate theoretical curves to compare against experimentally observed data. Figure 2(b) displays two theoretical curves: the red line calculated with silicon's dielectric parameters $\epsilon' = 16.3$ and $\epsilon'' = 0.3$, and the black dashed–dotted line, for which we completely eliminated the dissipative part, $\epsilon'' = 0$ in calculations. The same distance $z = 0.007\lambda_0$ from the dipole to the top surface of the structure was used. A good agreement between major features of the experimental data and the red theoretical curve is evident over the whole range of the spacer thicknesses. It is also transparent that there is no practical difference between red and black theoretical curves for spacers thicker than approximately 10–15 nm. The nonradiative contribution, Eq. (7), is therefore negligible for thicker spacers and the decay rate is entirely determined by radiative processes (5) and (6). As another qualitative confirmation, experimental lifetimes with thicker spacers clearly exhibit an oscillatory behavior in Fig. 2(b) characteristic of the radiative processes and related to interference effects [5,17].

For thin spacers, however, the difference between red and black theoretical curves can become very substantial, see the inset in Fig. 2(b). In this region, only the red theoretical curve agrees well with the pattern of the observed lifetimes. At these distances from the Si material, therefore, NRET from NQDs into Si, contribution (7), plays a significant role. In fact, for proximal NQDs grafted directly on the Si surface, NRET is a dominating decay process. Indeed, if one were to take the theoretical estimate for the radiative decay time $\tau_{rad} \simeq 5.1$ ns of proximal NQDs from the inset in Fig. 2(b) and compare it to the measured lifetime $\tau_{Si} \simeq 1.7$ ns, NRET would constitute a $1 - \tau_{Si}/\tau_{rad} \simeq 67\%$ fraction of the total decay rate. It is common to represent the NRET rate to a bulk layer of acceptors at distance r from the dipole in the form

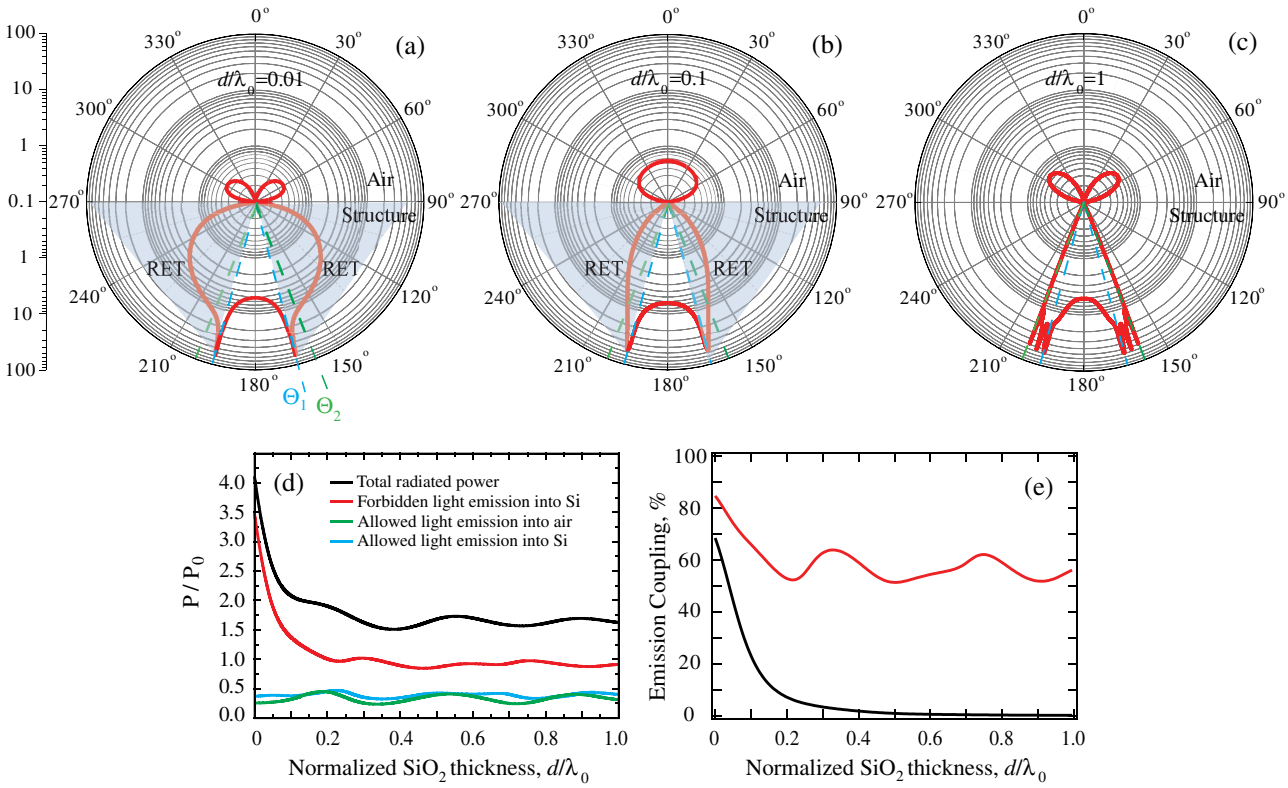

Fig. 3. Details of purely radiative decay processes for a randomly oriented NQD dipole at distance $z = 0.007\lambda_0$ from the surface of the SiO_2 spacer layer for different thicknesses d/λ_0 of the spacer. Panels (a)–(c) show the radiative emission patterns into the top [air, Eq. (8)] and bottom [Si, Eq. (9)] semi-spaces: (a) for $d/\lambda_0 = 0.01$, (b) $d/\lambda_0 = 0.1$, and (c) $d/\lambda_0 = 1$. Panel (d) displays the total radiated power (black curve) and contributions to it as integrated over appropriated ranges of emission angles. The green curve shows the power emitted into the air, the cyan curve the power emitted into Si via the "allowed light," that is, within angle θ_1 from the downward vertical direction. The red curve shows the power emitted into Si via the "forbidden light," that is, at angles beyond $\theta_1(\simeq 14.3°)$ from the downward direction. The latter emission corresponds to RET region shaded in blue in panels (a) and (b). Panel (e) displays proportions of the forbidden light emission in the total radiated power. The red curve corresponds to the emission into Si integrated over all angles beyond θ_1 from the downward direction. The black line shows the emission integrated over angles beyond $\theta_2(\simeq 21.8°)$ from the downward direction (angles between θ_1 and θ_2 excluded).

$\Gamma_{NRET}/\Gamma_0 = (R_0/r)^3$ referring to distance R_0 at which the NRET rate becomes equal to radiative decay rate (1) in vacuum. If we were to apply this relationship to the proximal NQDs with $r \simeq 4$ nm and using estimated $\tau_{NRET} \simeq 2.55$ ns and $\tau_0 \simeq 21.3$ ns (from measurements on the glass reference), R_0 would be roughly estimated as 8 nm for this emission wavelength. This estimate from proximal NQDs does not take into account extra dielectric screening due to spacers and/or the medium containing NQDs. In terms of the relationship to actual radiative processes, it is also important to keep in mind that the latter themselves are substantially accelerated in the vicinity of the high-refractive-index Si material and may therefore dominate over NRET at distances $r = R_0$.

A more detailed look into radiative processes is facilitated by theoretical illustrations in Fig. 3. Panels (a)–(c) of this figure show how substantially the radiative emission pattern can vary as a function of the SiO_2 spacer thickness. A common feature of all patterns, however, is that radiation into the Si semi-space dominates over radiation into the air semi-space. This domination is particularly significant for thinner, $d/\lambda_0 \lesssim 0.1$, spacers, as shown quantitatively via the integrated results in panel (d). While the emission of the "forbidden light," Eq. (6), of course takes place only into the Si semi-space, the "allowed light," Eq. (5), is emitted into both air and Si. Panel (d) shows that their relative amounts are comparable to each other but overall suppressed with respect to the power emitted in vacuum. The forbidden light emission due to the evanescent fields is, on the contrary, enhanced with respect to the emission in vacuum and constitutes the major contribution to the radiative decay. The electromagnetic modes radiated into Si will eventually get absorbed producing electron-hole pairs and realizing thus radiative ET from NQD excitons into Si. In thin Si films (as opposed to bulk Si), the absorption of "allowed" photons would be only partial, while the "forbidden" photons do not leave Si and propagate along Si slabs as waveguiding modes. That is why we chose to define RET for our applications as only due to radiation involving evanescent fields [11,12], as is shown schematically in panels (a) and (b). The red line in panel (e) displays the proportion of so defined RET in the total radiated power. For very thin spacers, this proportion is largely determined by the high index n of Si as the direct coupling of the NQD dipole and the evanescent fields of Si-based propagating modes ("tunneling" through the spacer) is efficient. The latter corresponds to the black curve in panel (e) that shows how this coupling becomes inefficient for thicker spacers. The proportion of RET for thick spacers is then determined by the refractive index n_G of SiO_2 and comparable to that on the reference glass. In other words, the integral (6) in this case is practically equal to $I(1, n_G)$. This is also nicely illustrated by panel (c) that shows that RET is practically limited to angles between critical θ_1 and θ_2 (no tunneling): photons radiated by the NQD into

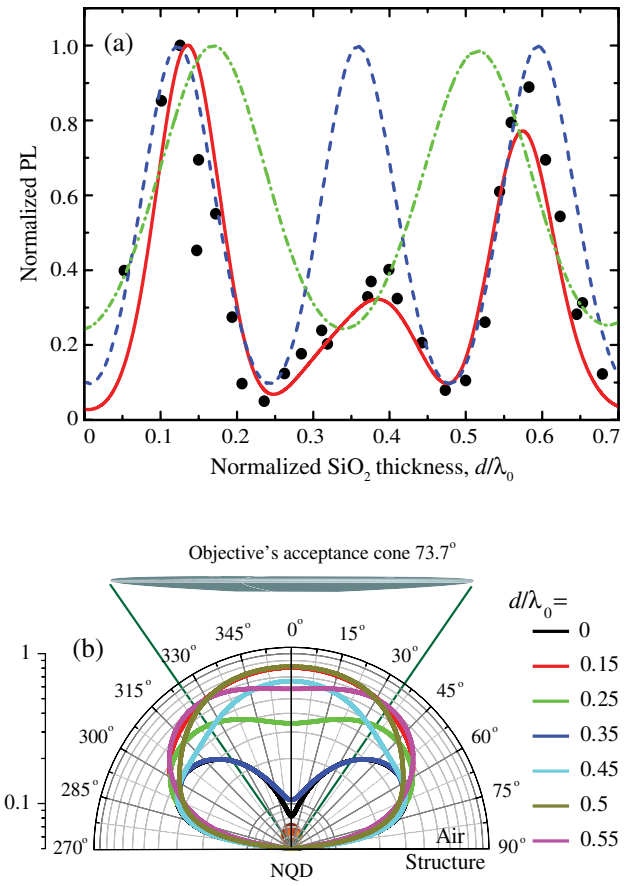

Fig. 4. (a) PL emission intensity from NQDs as a function of the thickness of the SiO_2 spacer layer. Black dots show experimental results as collected. The green dashed–dotted line shows the variation of the emitted power per one NQD exciton following from the integration of corresponding radiation patterns in panel (b) over objective's acceptance cone. The blue dashed line shows the variation of the intensity of the excitation laser field ($\lambda_{exc} = 400$ nm) at NQD positions reflecting thus the number of photogenerated excitons. The red line is a normalized product of the green and blue curves that is compared to the experimental data points. (b) PL emission patterns for several spacer thicknesses as indicated along with the collection cone of the objective used in experiments.

the spacer propagate there in various directions before refracting into Si according to the usual rules.

The time-resolved PL decay measurements require the use of pulsed lasers and TCSPC equipment. A much more common method, often used in sm-FRET studies, is to monitor PL intensity quenching of energy donors as a function of the separation distance from acceptor(s). The latter measurements can be implemented with continuous-wave (cw) lasers and even with fluorescence lamps as excitation sources. In our experiments, we monitored PL emission intensity along with the time-resolved traces. Black dots in Fig. 4(a) show the experimental data for integrated PL emission intensity as collected by our microscope objective with the aperture angle of about 73.7°. We already illustrated the variation of PL patterns (8) in Fig. 3, and more examples are provided in panel (b) of Fig. 4. Upon integration of the directed emitted power over the shown objective's cone, one arrives at the result displayed in Fig. 4(a) as the green dashed–dotted curve. This curve exhibits a substantial periodic modulation similar to the modulation for the green curve in Fig. 3(d) and reflecting the interference effects due to the spacer thickness. The discrepancy between the green curve and the experimentally observed pattern is evident.

It is important to recognize at this point that the theoretical green-curve results show the modulation of the PL intensity per one NQD exciton. The number of the photogenerated NQD excitons, however, depends on the intensity of the laser excitation field at NQD positions, which in turn is modulated in our SiO_2 – Si structures due to interference. The corresponding excitation modulation pattern calculated for our laser's $\lambda_{exc} = 400$ nm is shown in Fig. 4(a) as the blue dashed curve. As expected, this pattern exhibits a pronounced minimum at $d = 0$ due to a destructive interference caused by a phase shift between incoming and reflected waves at the high refractive index Si surface. The minimum is then periodically repeated consistently with the excitation wavelength inside the spacer. The superposition of the excitation and the emission profiles (the normalized product of the blue and green curves) is shown as the red line in Fig. 4(a) and agrees rather well with the trends displayed by the experimental data. We thus conclude that measurements of PL intensity quenching in the vicinity of multilayered dielectric structures are strongly affected by the specifics of the excitation and emission patterns and therefore need to be carefully analyzed for extraction of the underlying exciton decay rates.

The overall good agreement seen in Figs. 2 and 4 between salient features of experimental observations and theoretical expectations is likely indicative of the basic adequacy of the simplest theoretical model we employed. We stress in this regard that we intentionally have not attempted here to do fitting of the experimental data by modifying model parameters or by extending the model, e.g., via integrating over the (quite narrow) emission line or with variable weights from different dipole orientations, etc. Our goal has rather been to rationalize the major trends observed in experimental data that would allow us to draw conclusions on the nature of ET processes from photoexcited NQDs into adjacent Si substrates. The rationalization achieved here and in our previous studies [10–12] further attests to the generality of macroscopic electrodynamics framework [5,17] developed for understanding of the environment-dependent electromagnetic decay rates.

4. CONCLUSIONS

In summary, we performed a combined experimental and computational study of the decay of photoexcitations in individual NQDs grafted on SiO_2 – Si substrates with a variable thickness of the SiO_2 spacer layer. The study involved both time-resolved PL kinetics and PL intensity quenching. We showed that the salient features of experimental observations can be well understood within the picture of the modification of spontaneous decay of electric-dipole excitons by their environment. The corresponding analysis of the experimental data reveals that ET from NQDs into substrates is a major enabler of substantial variations in spontaneous decay rates. We have demonstrated that while time-resolved PL kinetics provides a direct access to the assessment of ET processes, PL intensity measurements can be affected by the specifics of the optical generation and emission collection and therefore need to be processed more carefully for interpretations.

Two distinct mechanisms of ET into Si can be identified to be at work in our experimental system. NRET is a major contributor for proximal NQDs in this spectral range ($\lambda_0 \simeq 565$ nm) but relinquishes its dominating role already at distances $\lesssim$10 nm from the Si surface. NRET corresponds to the direct production of electron-hole pairs in Si and its rate is ultimately tied to the magnitude of the imaginary part ϵ'' of silicon's dielectric function. Radiative ET (RET), on the other hand, relies on the real part ϵ' of the dielectric function and is an efficient process thanks to a high refraction index $n \simeq 4$ of Si. In RET process, the exciton preferentially decays into electromagnetic modes propagating only in the substrate. The efficient direct coupling of NQD excitons to Si-based modes takes place at distances $\lesssim 0.1\lambda_0$ making it a much longer range process than NRET. RET is even longer-ranged when assisted by propagation in the spacer layer. For thin-film substrates, RET results in the excitation of waveguiding modes. Effective RET coupling was in fact recently demonstrated in time-resolved PL decay measurements for NQDs grafted onto ultrathin Si nanomembranes [11]. Waveguiding modes would propagate along the film getting eventually absorbed and producing electron-hole pairs in addition to those due to NRET. The demonstrated high efficiency of ET into Si therefore supports the concept of hybrid PV devices where thin Si films are sensitized by ET from adjacent layers of absorbing materials.

Given the spectral behavior of silicon's $\epsilon(\omega)$, the relative role of RET in overall ET actually increases toward the near-IR region of the spectrum [12]. "Funneling" of emitter's dipolar radiation into high-index substrates [29,30], which is the basis of efficient RET we discussed, can also be used for various optical applications. Recently, e.g., such an approach had been successfully applied to greatly enhance the collection efficiency from single molecules embedded in an organic layer on top of the sapphire substrate [31]. Collection of the emitted photons in this case is accomplished via high-NA immersion objective positioned below the bottom of the sapphire substrate, that is, employing photons preferentially out-coupled through the substrate.

ACKNOWLEDGMENTS

This work was supported by NSF (DMR-1207123) and partly by NSF (CHE-0911197) and the Texas Higher Education Coordinating Board NHARP Programs.

REFERENCES

1. J. R. Lakowicz, *Principles of Fluorescence Spectroscopy* (Springer, 2006).
2. Y. Sun, H. Wallrabe, S. Seo, and A. Periasamy, "FRET microscopy in 2010: the legacy of Theodor Förster on the 100th anniversary of his birth," ChemPhysChem **12**, 462–474 (2011).
3. A. R. Clapp, I. L. Medintz, and H. Mattoussi, "Förster resonance energy transfer investigations using quantum-dot fluorophores," ChemPhysChem **7**, 47–57 (2006).
4. V. May and O. Kühn, *Charge and Energy Transfer Dynamics in Molecular Systems* (Wiley-VCH, 2004).
5. L. Novotny and B. Hecht, *Principles of Nano-Optics* (Cambridge University, 2006).
6. R. F. Oulton, N. Takada, J. Koe, P. N. Stavrinou, and D. D. C. Bradley, "Strong coupling in organic semiconductor microcavities," Semicond. Sci. Technol. **18**, S419–S427 (2003).
7. V. M. Agranovich, Y. N. Gartstein, and M. Litinskaya, "Hybrid resonant organic-inorganic nanostructures for optoelectronic applications," Chem. Rev. **111**, 5179–5214 (2011).
8. S. Chanyawadee, R. T. Harley, M. Henini, D. V. Talapin, and P. G. Lagoudakis, "Photocurrent enhancement in hybrid nanocrystal quantum-dot *p-i-n* photovoltaic devices," Phys. Rev. Lett. **102**, 077402 (2009).
9. S. Lu, Z. Lingley, T. Asano, D. Harris, T. Barwicz, S. Guha, and A. Madhukar, "Photocurrent induced by nonradiative energy transfer from nanocrystal quantum dots to adjacent silicon nanowire conducting channels: toward a new solar cell paradigm," Nano Lett. **9**, 4548–4552 (2009).
10. H. M. Nguyen, O. Seitz, D. Aureau, A. Sra, N. Nijem, Y. N. Gartstein, Y. J. Chabal, and A. V. Malko, "Spectroscopic evidence for nonradiative energy transfer between colloidal CdSe/ZnS nanocrystals and functionalized silicon substrates," Appl. Phys. Lett. **98**, 161904 (2011).
11. H. M. Nguyen, O. Seitz, W. Peng, Y. N. Gartstein, Y. J. Chabal, and A. V. Malko, "Efficient radiative and nonradiative energy transfer from proximal CdSe/ZnS nanocrystals into silicon nanomembranes," ACS Nano **6**, 5574–5582 (2012).
12. M. Nimmo, L. Caillard, W. DeBenedetti, H. M. Nguyen, O. Seitz, Y. N. Gartstein, Y. J. Chabal, and A. V. Malko, "Visible to near infrared sensitization of silicon substrates via energy transfer from proximal nanocrystals: Further insights for hybrid photovoltaics," ACS Nano **7**, 3236–3245 (2013).
13. L. Gaudreau, K. J. Tielrooij, G. E. D. K. Prawiroatmodjo, J. Osmond, F. J. G. de Abajo, and F. H. L. Koppens, "Universal distance-scaling of nonradiative energy transfer to graphene," Nano Lett. **13**, 2030–2035 (2013).
14. D. L. Dexter, "Two ideas on energy transfer phenomena: ion-pair effects involving the OH stretching mode, and sensitization of photovoltaic cells," J. Lumin. **18/19**, 779–784 (1979).
15. A. L. Rogach, T. A. Klar, J. M. Lupton, A. Meijerink, and J. Feldman, "Energy transfer with semiconductor nanocrystals," J. Mater. Chem. **19**, 1208–1221 (2009).
16. M. Stavola, D. L. Dexter, and R. S. Knox, "Electron-hole pair excitation in semiconductors via energy transfer from an external sensitizer," Phys. Rev. B **31**, 2277–2289 (1985).
17. R. R. Chance, A. Prock, and R. Silbey, "Molecular fluorescence and energy transfer near interfaces," in *Advances in Chemical Physics*, S. A. Rice and I. Prigogine, eds. (Wiley, 1978), Vol. **37**, pp. 1–65.
18. V. M. Agranovich and M. D. Galanin, *Electronic Excitation Energy Transfer in Condensed Matter* (Elsevier, 1982).
19. D. E. Aspnes and A. A. Studna, "Dielectric functions and optical parameters of Si, Ge, GaP, GaAs, GaSb, InP, InAs, and InSb from 1.5 to 6.0 eV," Phys. Rev. B **27**, 985–1009 (1983).
20. A. P. Alivisatos, M. F. Arndt, S. Efrima, D. H. Waldeck, and C. B. Harris, "Electronic energy transfer at semiconductor surfaces. I. Energy transfer from two-dimensional molecular films to Si (111)," J. Chem. Phys. **86**, 6540–6549 (1987).
21. L. A. Blanco and F. J. G. de Abajo, "Spontaneous light emission in complex nanostructures," Phys. Rev. B **69**, 205414 (2004).
22. O. Seitz, M. Dai, F. S. Aguirre-Tostado, R. M. Wallace, and Y. J. Chabal, "Copper-metal deposition on self assembled monolayer for making top contacts in molecular electronic devices," J. Am. Chem. Soc. **131**, 18159–18167 (2009).
23. D. Aureau, Y. Varin, K. Roodenko, O. Seitz, O. Pluchery, and Y. J. Chabal, "Controlled deposition of gold nanoparticles on well-defined organic monolayer grafted on silicon surfaces," J. Phys. Chem. C **114**, 14180–14186 (2010).
24. O. Seitz, P. G. Fernandez, G. A. Mahmud, H.-C. Wen, H. J. Stiegler, R. A. Chapman, E. M. Vogel, and Y. J. Chabal, "One-step selective chemistry for silicon-on-insulator sensor geometries," Langmuir **27**, 7337–7340 (2011).
25. A. Sommerfeld, "Über die ausbreitung der wellen inder drahtlosen telegraphie," Ann. Phys. Lpz. **81**, 1135–1153 (1926).
26. A. Sommerfeld, *Partial Differential Equations in Physics* (Academic, 1964).
27. D. H. Waldeck, A. P. Alivisatos, and C. B. Harris, "Nonradiative damping of molecular electronic excited states by metal surfaces," Surf. Sci. **158**, 103–125 (1985).
28. W. Lukosz, "Light emission by magnetic and electric dipoles close to a plane dielectric interface. III. Radiation patterns of dipoles with arbitrary orientation," J. Opt. Soc. Am. **69**, 1495–1503 (1979).

29. L. Luan, P. R. Sievert, B. Watkins, W. Mu, Z. Hong, and J. B. Ketterson, "Angular radiation pattern of electric dipoles embedded in a thin film in the vicinity of a dielectric subspace," Appl. Phys. Lett. **89**, 031119 (2006).
30. L. Luan, P. R. Sievert, and J. B. Ketterson, "Near-field and far-field electric dipole radiation in the vicinity of a planar dielectric half space," New J. Phys. **8**, 264 (2006).
31. K. G. Lee, X. W. Chen, H. Eghlidi, P. Kukura, R. Lettow, A. Renn, V. Sandoghdar, and S. Götzinger, "A planar dielectric antenna for directional single-photon emission and near-unity collection efficiency," Nat. Photonics **5**, 166–169 (2011).